Environmental Processes (2024) 11:49
https://doi.org/10.1007/s40710-024-00726-2

RESEARCH

# Competitive Adsorption of 4-Hydroxybenzaldehyde and Toluene onto High Silica Zeolites

**Tatiana Chenet[1] · Maura Mancinelli[2] · Elena Sarti[3] · Valentina Costa[1] · Caterina D'Anna[1] · Annalisa Martucci[2] · Luisa Pasti[1]**

Received: 21 March 2024 / Accepted: 15 August 2024


## Abstract

To evaluate the ability of zeolites to remove natural low molecular organic substances, p-hydroxybenzaldehyde (p-HBA), a phenolic compound derived from lignin, was chosen as a representative of naturally occurring dissolved organic substances. Two distinct high-silica zeolite materials, namely ZSM-5 and Y, were utilised for the study, and the adsorption process was investigated under a wide range of conditions. It has been observed that p-HBA is adsorbed by both zeolites, and the pH significantly impacts the adsorption of p-HBA, particularly within the low concentration range, while exerting minimal influence on the saturation capacity. For both zeolites, various isotherm models were assessed to accurately describe the adsorption data obtained from aqueous solutions of p-HBA. In addition, to comprehend the selectivity of the adsorbents towards natural organic substances and xenobiotics, the competitive adsorption of mixtures of p-HBA and toluene (TOL) was investigated. The zeolite's saturation capacity for p-HBA diminishes with increasing contaminant concentration. Conversely, the adsorption of toluene remains minimally affected by p-HBA, and it has been demonstrated that toluene can displace adsorbed p-HBA from the zeolites' sites. This finding has been confirmed by diffractometric study that indicates that TOL and p-HBA occupy "the same" adsorption sites. Furthermore, Rietveld refinements reveal the formation of p-HBA complexes interacting with the framework and stabilising the guest structures within the zeolite porosity. The results obtained are important for the selection of proper adsorbent for the removal of hydrocarbons in environmental application (natural waters).

✉ Luisa Pasti
luisa.pasti@unife.it

[1] Department of Environment and Prevention Sciences, University of Ferrara, Via Borsari, 46, Ferrara 44121, Italy

[2] Department of Physics and Earth Science, University of Ferrara, Via Saragat, 1, Ferrara 44122, Italy

[3] Department of Chemical, Pharmaceutical and Agricultural Sciences, University of Ferrara, Via Borsari, 46, Ferrara 44121, Italy

Published online: 02 September 2024

**Highlights**

- ZSM-5 and Y high silica zeolites adsorb p-HBA, and the adsorption is influenced by pH.
- ZSM-5 and Y high silica zeolites exhibit higher selectivity for toluene compared to p-HBA.
- Toluene and p-HBA compete for occupancy sites within the frameworks of both zeolites.
- Toluene can displace p-HBA molecules from the pores of the zeolite.

**Keywords** Organic Contaminants · Lignin Derived Phenolic Compounds · Zeolites · Water Remediation · Competitive Adsorption

## 1 Introduction

Natural organic matter (NOM) is ubiquitous in surface and groundwaters. NOM is a complex mixture of organic molecules with varying structures and compositions, and it exists in particulate, colloidal, and dissolved forms (Beckett and Ranville 2006; Matilainen et al. 2011). Its presence in raw water can affect treatment and remediation processes; generally, increasing NOM concentration increases the demand for chemical coagulants and disinfectants (Jacangelo et al. 1995). Particularly, the colloidal and dissolved forms pose more challenges in water treatment processes, as some of these substances can interact with organic compounds and metals, enhancing their mobility through the purification system. Moreover, during potabilization processes, hazardous disinfection by-products (DBPs) can form when NOM is present in the water matrix. Both halogenated and nonhalogenated DBPs may arise from the degradation of NOM. It is well known that many halogenated DBPs are considered harmful even at low concentrations, and trihalometanes (THMs) have been classified as probable and possible human carcinogens (IARC 1999). Due to their potential risk to public health, various strategies have been proposed for reducing halogenated DBPs in chlorinated drinking waters. To evaluate potential removal methodologies, halogenated DBPs precursors must be identified and the mechanism through which THMs form during chlorination of NOM must be elucidated. Studies have been conducted to model DBP formation from different NOM compositions during chlorination (Mitch et al. 2023; Hincapié–Upegui et al. 2024).

Recently, it has been reported that a new approach based on chlorine disinfection followed by Granulated Activated Carbon (GACs) adsorption of DBPs is capable of reducing the concentration of chlorinated toxic compounds in treated water by approximately 51%, with a decrease of cytotoxic and genotoxic potential of the treated waters up to 83% (Jiang et al. 2020).

Many of the nonhalogenated DBPs, such as the lignin derived phenolic compounds, occur naturally in surface and groundwater resulting from degradation of biomasses; moreover, they can also be found in natural water from the discharge of industrial wastewaters, especially those deriving from different papermaking process stages, including pulping, bleaching, and washing. Indeed, their interference in remediation processes based on adsorption (Pignatello et al. 2006; Molé et al. 2024) and oxidation (Zhu et al. 2022; Mathew et al. 2024) has been extensively reported. It has been reported that lignin derived phenolic compounds such as para hydroxybenzaldehyde can be the precursor of halogenated DBPs (Jiang et al. 2020). Therefore, it is important to investigate the interaction of lignin derived compounds with adsorbent materials for a double purpose: on one hand to determine the efficiency of the adsorbents to extract these natural compounds from water

preventing the formation of halogenated DBPs during chlorination treatments, and on the other hand to comprehend their selectivity towards dissolved organic substances and xenobiotics to assess the reliability of absorption-based remediation technology (Amrutha et al. 2023; Parniske et al. 2024).

Zeolites have been investigated to eliminate emerging contaminants, including pesticides, pharmaceuticals, and perfluorinated compounds from aqueous matrices (Chi et al. 2022; Mancinelli et al. 2022; Pérez-Botella et al. 2022; Abas and Fathy 2024; Almuhtaseb et al. 2024). Previous studies confirmed that some monomers of humic acids can compete with contaminants for adsorption sites (Zuo et al. 2020; Wang et al. 2024). Meanwhile, complex interactions could be established between organic contaminants and dissolved organic molecules of natural origin which could influence contaminants adsorption (Braschi et al. 2016). However, only few works investigate the adsorption of monomers of humic acids onto zeolites (Braschi et al. 2016; Chenet et al. 2020; Chi et al. 2022). Additionally, since these substances occur simultaneously with other contaminants in natural and wastewaters, they can also interact with each other and may show synergistic or antagonistic behaviour during adsorption.

In the present study the adsorption of one of the nonhalogenated DBPs, 4-hydroxybenzaldheyde (p-HBA), onto two different high-silica zeolites (HSZs), Y and ZSM-5, was investigated in a wide range of conditions. The two selected adsorbents are characterised by different structures, MFI-type and FAU-type framework topology for ZSM-5 and Y, respectively (Baerlocher et al. 2007). Moreover, the two materials differ in the dimensions of the opening window; specifically, ZSM-5 is a medium pore material, whereas zeolite Y is a large pore adsorbent with cavities known as "supercages". The comparison of the adsorption properties of the two zeolites was carried out to assess the role of pore size and the framework structure. Additionally, to evaluate the selectivity of the selected adsorbents, a comparison between the adsorption of p-HBA from aqueous matrices with or without the presence of the contaminant toluene (TOL) was performed. Moreover, a structural investigation was carried out to study the possible interactions between the adsorbates (TOL, p-HBA and water) and the framework of the zeolites through the localisation of the molecules within the zeolite pores.

To enhance the design of reliable adsorbents and the configuration of adsorption systems, it is essential to study the multi-component adsorption process, as highlighted in a recent review (Amrutha et al. 2023). Therefore, the present work contributes to global efforts to improve the efficiency and safety of water treatment processes. To the best of our knowledge, no research has been conducted on the utilisation of zeolites as an adsorbent for the removal of p-HBA and p-HBA and TOL mixtures from aqueous matrices.

## 2 Materials and Methods

In the present study, for the preparation of solutions used in the adsorption investigation and for the mobile phase used for the analyses by high performance liquid chromatography, reagents characterised by a purity grade > 99.8% were used (for the complete list see the section *Chemicals* in the Supplementary Material).

The zeolites utilised in this work were high silica ZSM-5, characterised by a silica to alumina ratio of 280, and Y, characterised by a silica to alumina ratio of 200 (see the section *Zeolites specifications* in the Supplementary Material (SM) for the detailed characteristics). Specific surface area (SSA), pore size distribution and XRD pattern of both zeolites

are reported in the Supplementary Material section (see Table SM1 and Figs. SM1 and SM2).

### 2.1 Batch Adsorption

The batch method was employed to perform the adsorption experiments as described by Chenet et al. (2020), using a solid to solution ratio of 1 mg to 2 mL, keeping the batch under stirring at room temperature for 24 h. After equilibration, the batch was filtered to separate the adsorbent from the solution; the concentrations of the target compounds in the aqueous phase were determined by high performance liquid chromatography equipped with a DAD UV-Vis detector (see the section *Batch method and HPLC-DAD instrumental conditions* in the Supplementary Material for the detailed description).

The adsorbed quantities, q (mg $g^{-1}$), were obtained as follows:

$$q = \frac{\left(C_0 - C_e\right) \cdot V}{m} \tag{1}$$

where $C_0$ (mg $L^{-1}$) is the initial concentration of p-HBA or TOL, whereas $C_e$ (mg $L^{-1}$) is the concentration at equilibrium, $m$ (g) is the quantity of adsorbent material, and $V$ (L) is the volume of the solution.

All experiments were performed in triplicates. Model equations (see Eq. 2 to 11 and 13) were used to fit the experimental kinetics and isotherm data; MATLAB® software was employed to evaluate all the parameters of the models through non-linear regression.

### 2.2 Thermal Analyses

A STA 409 PC LUXX thermal analyser (Netzsch, Germany) working with a heating rate of 10 °C $min^{-1}$ from room temperature up to 900 °C and with a 20 mL $min^{-1}$ $N_2$ flow rate, was employed for thermogravimetric (TG) and differential thermal analysis (DTA) measurements of ZSM-5 and Y zeolite samples loaded with the targeted compounds after adsorption.

### 2.3 X-ray Powder Diffraction (XRPD) Measurements and Refinement Procedure

Room temperature XRPD patterns collection by conventional radiation of both p-HBA-loaded and p-HBA-TOL-loaded ZSM-5 and Y were performed with a D8 Advance diffractometer (Bruker AXS, Madison, WI, USA) provided with a Si(Li) solid state detector (Sol-X). The experimental settings were: Cu $K\alpha_1,\alpha_2$ radiation ($\lambda = 1.54178$ Å), 2θ range 3-110°, step size 0.02°, time/step 12 s, scattering, divergence, and receiving slits 0.6, 0.6 and 0.1 mm, respectively. Structural refinements were carried out by full profile Rietveld analysis using the GSAS package (Larson and Von Dreele 2004) with the EXPGUI interface (Toby 2001). The atomic coordinates reported by Rodeghero et al. (2016) and Chenet et al. (2020) for the ZSM-5 and Y framework atoms were used as guess models. Specific details on the refinement strategy and data on selected bond distances (Å) and angles (◦) between framework and extraframework atoms for both Y–p-HBA and ZSM-5– p-HBA systems are reported in the Supplementary Material. Refined atomic coordinates, occupancies, and isotropic thermal parameters for both loaded zeolites are listed in Tables SM2 and SM3.

## 3 Results and Discussion

### 3.1 Adsorption Kinetics

The uptake process of organic contaminants, such as toluene, chlorobenzene, 1–2 dichoroethane and methyl tert-butyl ether on zeolites from unary aqueous solutions has been extensively studied (Rodeghero et al. 2017; Pasti et al. 2018; Almuhtaseb et al. 2024). In this work, before the investigation of possible competition between TOL and p-HBA, a thorough study of the uptake of the lignin derived compound on both zeolites was carried out.

To describe the adsorption kinetic process several adsorption kinetic models can be employed, including the pseudo-first-order (PFO) (Lagergren 1898), the pseudo-second-order (PSO) (Ho 2006), the phenomenological mass transfer (Marin et al. 2014; Monte Blanco et al. 2017; Scheufele et al. 2016; Suzaki et al. 2017), the Elovich (Elovich and Larinov 1962), and the mixed-order (MO) (Guo and Wang 2019) models.

The PFO model (Lagergren 1898) in its integrated form, by assuming $q_0 = 0$, is given by

$$q_t = q_e\left(1 - e^{-k_1 t}\right) \tag{2}$$

where $q_t$ (mg $g^{-1}$) is the adsorbed quantity per unit mass of adsorbent at time $t$ (min), $q_e$ (mg $g^{-1}$) is the equilibrium adsorption quantity assessed by the PFO model, and $k_1$ ($min^{-1}$) is the pseudo-first-order kinetic constant, which has been used to indicate the velocity to reach the adsorption equilibrium (Plazinski et al. 2009). The model has been extensively employed to describe the kinetic data and to obtain the $q_e$ and $k_1$ parameters. Another model that has been widely employed to describe the adsorption processes is the PSO model (Ho 2006), which is described according to the following equation:

$$q_t = \frac{k_2\, q_e^2\, t}{1 + k_2\, q_e\, t} \tag{3}$$

where $k_2$ (g $mg^{-1}$ $min^{-1}$) is the pseudo-second-order kinetic constant.

The Weber-Morris (W&M) has been employed to investigate the rate controlling step, and in particular the role of intraparticle diffusion in adsorption kinetics. The W&M model can be described as follows:

$$q_t = k_D\, t^{\frac{1}{2}} + C \tag{4}$$

where $k_D$ (mg $g^{-1}$ $min^{-1/2}$) is the diffusion coefficient in the solid, and $C$ (mg $g^{-1}$) is related to the boundary layer thickness.

The Elovich model, which can be related to the model of a strongly heterogeneous solid surface (Plazinski et al. 2009), is expressed as follows:

$$q_t = \left(-\frac{1}{\beta}\right)\left(ln(\alpha\,\beta) + ln\left(t + \frac{1}{\alpha\,\beta}\right)\right) \tag{5}$$

where $\beta$ (g $mg^{-1}$) is a constant related to the surface coverage and $\alpha$ (mg $g^{-1}$ $min^{-1}$) is the rate constant of chemisorption (McLintock 1967). The Elovich kinetic model was developed and has been used to describe the adsorption of gases onto solids, but it has also been successfully applied to liquid/solid systems (Cheung et al. 2001; Fuentes et al. 2014).

The uptake of p-HBA onto ZSM-5 and Y zeolites was measured at three different concentrations. From preliminary adsorption data, Y zeolites did not show appreciable adsorption from diluted solutions. For this reason, the reported kinetic curves of Y zeolite refer to higher concentrations with respect to those employed for ZSM-5; in addition, since pH can influence the adsorption (see Sect. 3.2.2 *pH influence*) the solution pH was kept constant for all the uptake experiments (pH 5). The experimental data are reported in Fig. 1.

Both zeolite ZSM-5 and Y show very fast kinetics with the equilibrium reached within the first 20 min of contact; the estimated parameters obtained from the kinetic models described above by interpolating the experimental data are summarised in Table 1.

The experimental data for both zeolites are well described with all the models ($R^2 > 0.98$) except the Weber and Morris model, which was used to fit the data in the early stage of the uptake process; in this case, the plot of $q_t$ versus $t^{1/2}$ show a linear trend, with intercept = 0 when the intraparticle diffusion is the main rate controlling step. The multilinear segments that compose the experimental data sets show that different mechanisms control the rate of adsorption for both zeolites. Since the coefficient of determination ($R^2$) obtained for the different kinetic models are quite close (between 0.98 and 0.99, without considering the W&M model), it is difficult to clearly identify the mechanism of adsorption. As can be seen from Table SM4 the difference between the estimated $q_e$ values and the measured $q_e$ from the isotherm determination experiments is negligible, indicating on one hand the goodness of the fitting using PFO and PSO models, but on the other hand, it does not allow to suggest one model over the other to better understand the mechanism involved.

Although some authors do not encourage to use linearisation for studying the kinetics of adsorption based on evidence that non-linear regression is a more robust and reliable tool for data modelling (González-López et al. 2022), the experimental data were fitted by using the linearised form of PFO and PSO (Fig. SM3). The results are reported in supplementary material (SM). By comparing the goodness of fitting of linearised models, it seems that the

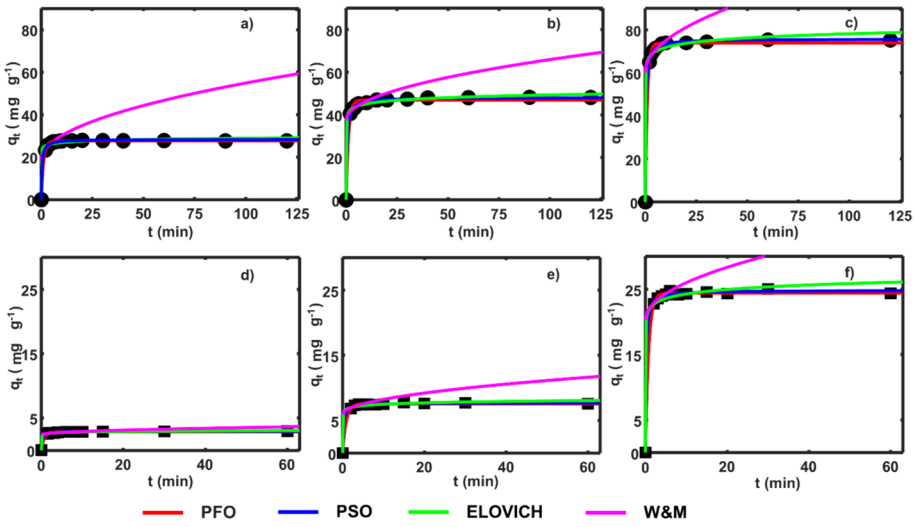


**Fig. 1** Kinetic experimental data fitted with PFO, PSO, Elovich and W&M kinetic models. a), b) and c): adsorption kinetics of p-HBA on Y zeolite (initial concentration: 40, 60, 80 mg L$^{-1}$, respectively); d), e) and f): adsorption kinetics of p-HBA on ZSM-5 (initial concentration: 5, 10, 20 mg L$^{-1}$, respectively)

**Table 1** Kinetic parameters, with confidence intervals at 95%, obtained with the adsorption kinetic models (eqs. 2–5) for zeolites ZSM-5 and Y at different initial p-HBA concentrations

| Kinetic model | | Zeolite Y | | | Zeolite ZSM-5 | | |
|---|---|---|---|---|---|---|---|
| | | p-HBA concentration (mg $L^{-1}$) | | | p-HBA concentration (mg $L^{-1}$) | | |
| | | 40 | 60 | 80 | 5 | 10 | 20 |
| PFO | $q_e$ | 27.62 ± 0.19 | 46.82 ± 0.92 | 73.85 ± 1.08 | 2.861 ± 0.059 | 7.567 ± 0.081 | 24.41 ± 0.22 |
| | $k_1$ | 0.8911 ± 0.063 | 0.8881 ± 0.17 | 0.9927 ± 0.14 | 1.455 ± 0.31 | 1.156 ± 0.16 | 1.292 ± 0.18 |
| | $R^2$ | 0.9982 | 0.9894 | 0.9969 | 0.9938 | 0.9978 | 0.9984 |
| | SSE | 1.31 | 21.33 | 15.01 | 0.0451 | 0.1143 | 0.8831 |
| PSO | $q_e$ | 28.27 ± 0.32 | 48.11 ± 0.29 | 75.69 ± 0.50 | 2.941 ± 0.032 | 7.728 ± 0.12 | 24.81 ± 0.31 |
| | $k_2$ | 0.1055 ± 0.024 | 0.053 ± 5.4e-03 | 0.04343 ± 5.3e-03 | 1.577 ± 0.32 | 0.6066 ± 0.24 | 0.2555 ± 0.10 |
| | $R^2$ | 0.9969 | 0.9993 | 0.9996 | 0.999 | 0.9975 | 0.9985 |
| | SSE | 2.182 | 1.341 | 1.907 | 0.007387 | 0.1293 | 0.8109 |
| Elovich | $\beta$ | 1.1075 ± 0.40 | 1.823 ± 0.42 | 2.753 ± 1.09 | 0.1268 ± 0.029 | 0.3158 ± 0.15 | 0.9936 ± 0.50 |
| | $\alpha$ | 7.1013e + 11 ± 1.57e + 12 | 1.0045e + 10 ± 5.51e + 09 | 5.9217e + 10 ± 2.15e + 10 | 7.0513e + 07 ± 2.86e + 09 | 6.4234e + 08 ± 2.32e + 10 | 4.0062e + 09 ± 4.93e + 10 |
| | $R^2$ | 0.9836 | 0.9952 | 0.993 | 0.9974 | 0.9904 | 0.9901 |
| | SSE | 11.66 | 9.6 | 33.84 | 0.01899 | 0.4973 | 5.324 |
| W&M | $k_D$ | 3.619 ± 1.84 | 2.847 ± 1.72 | 4.693 ± 2.31 | 0.1547 ± 0.071 | 0.7416 ± 1.32 | 1.792 ± 0.58 |
| | $C$ | 18.74 ± 3.67 | 37.5 ± 3.85 | 60.16 ± 5.32 | 2.438 ± 0.14 | 5.901 ± 2.48 | 20.32 ± 1.15 |
| | $R^2$ | 0.9291 | 0.8405 | 0.8887 | 0.9024 | 0.7436 | 0.9703 |
| | SSE | 0.6664 | 2.859 | 6.053 | 0.004879 | 0.07118 | 0.06562 |

PSO model better describes the experimental data. However, it should be considered that it is not recommended to compare the values of $R^2$ of linearised PFO and PSO models (Lima et al. 2021; Bujdák 2020), and that the mentioned expressions (e.g., PFO and PSO) do not correspond to only one kinetic model, but they are equations able to simulate adequately well the behaviour characteristic of physical kinetic processes of various kinds (Plazinski et al. 2009). Consequently, it is difficult to state what kind of process governs the sorption kinetics based on small differences in the determination coefficient.

## 3.2 Adsorption of p-HBA on ZSM-5 and Y Zeolites

### 3.2.1 Adsorption Isotherms

The adsorption isotherms of p-HBA on ZSM-5 and Y zeolites are presented in Fig. 2.

The most common adsorption isotherm models have been used to fit the experimental data to elucidate the mechanism of the p-HBA uptake process.

The Langmuir isotherm model is described as follows:

$$q_e = \frac{q_s\, b\, C_e}{1 + b\, C_e} \tag{6}$$

where $q_e$ (mg $g^{-1}$) is the quantity of p-HBA adsorbed onto the zeolite at equilibrium, $C_e$ (mg $L^{-1}$) is the concentration of p-HBA in the aqueous phase at equilibrium, $q_s$ (mg $g^{-1}$) represents the saturation capacity, $b$ is a constant associated to the binding affinity (L $mg^{-1}$). The Langmuir adsorption isotherm model assumes a homogeneous monolayer formation with adsorption sites energetically identical, with no lateral interactions and steric hindrance between the adsorbed molecules (Foo and Hameed 2010). This model has been widely employed for the description and comparison of the adsorption capacity of many adsorbent materials towards several substances (Park et al. 2014; Ma et al. 2015; Turk Sekulic et al. 2019; Mancinelli et al. 2022).

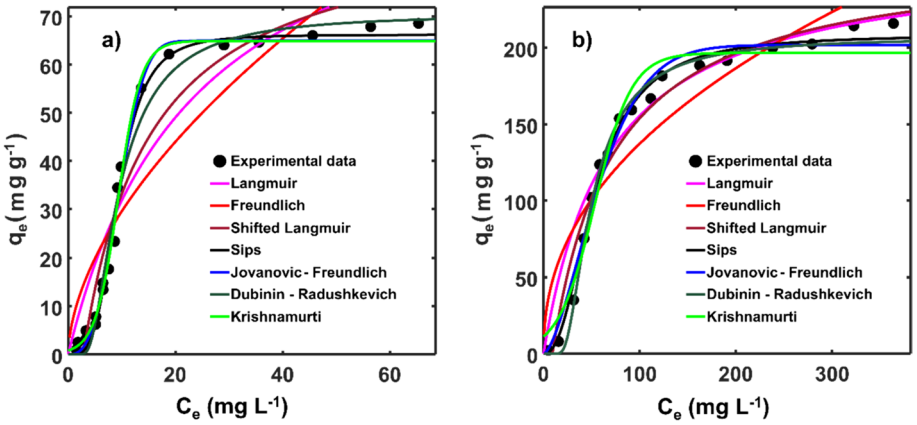


**Fig. 2** Isotherm experimental data fitted with Langmuir, Freundlich, Shifted Langmuir, Sips, Jovanovic-Freundlich, Dubinin-Radushkevich and Krishnamurti adsorption isotherm models. (a) adsorption isotherm of p-HBA onto ZSM-5, (b) adsorption isotherm of p-HBA onto Y zeolite

The shifted Langmuir isotherm model is a variation of the Langmuir model described above, which can be described by the following form:

$$q_e = \frac{q_s\, b_{sh}\, (C_e - C_{sh})}{1 + b_{sh}\, (C_e - C_{sh})} \tag{7}$$

where $C_{sh}$ is the concentration shift on the x-axis (mg $L^{-1}$) which is subtracted from the concentration of solute in the solution at equilibrium ($C_e$), and $b_{sh}$ (L $mg^{-1}$) is the corresponding affinity constant. This model can be applied to S-shaped isotherms assuming a cooperative adsorption process; in this regard, the concentration of the shift can be assumed to be the minimum quantity in solution needed for the adsorption to promptly occur (Grant et al. 1998).

The Freundlich isotherm model is expressed as indicated by Eq. (8):

$$q_e = K_F C_e^{\frac{1}{n}} \tag{8}$$

where $K_F$ is the Freundlich isotherm constant related to the adsorption capacity (mg $g^{-1}$)(L $g^{-1}$)$^n$, and *1/n* identifies the adsorption intensity of the adsorbate onto the adsorbent (when $n > 1$ the adsorption is achieved under favourable conditions). This model is not restricted to monolayer formation, it assumes a multilayer adsorption, with a non-uniform distribution of adsorption energies and affinities on the heterogeneous surface. The slope of the curve gives a measure of the intensity of the adsorption or the heterogeneity of the surface; in particular, when this parameter approaches 0 the adsorption becomes more heterogeneous (Foo and Hameed 2010).

The Sips isotherm model is described by Eq. (9):

$$q_e = \frac{q_s\, b_s\, C_e^{\beta_s}}{1 + b_s\, C_e^{\beta_s}} \tag{9}$$

with $b_s$ (L $mg^{-1}$) representing the constant related to the adsorption equilibrium, whereas $\beta_s$ is a constant characteristic of the adsorption system (when $\beta_s$ equals 1, Sips equation becomes the Langmuir model).

This equation is a combination of the Langmuir and Freundlich models: at low adsorbate concentrations, it follows the Freundlich model, while at high adsorbate concentrations it describes a monolayer adsorption capacity according to the Langmuir model (Foo and Hameed 2010; Günay et al. 2007).

Equation (10) describes the Jovanovich-Freundlich (J-F) adsorption isotherm model:

$$q_e = q_s\left(1 - e^{-(aC_e)^{\nu}}\right) \tag{10}$$

where $\nu$ is a parameter which accounts for surface heterogeneity and $a$ (L $mg^{-1}$) is a temperature-dependent parameter related to the interaction energy distribution. This model can be applied to describe experimental data related to single-component adsorption equilibria on heterogeneous materials (Quiñones et al. 1996).

Equation (11) describes the Dubinin-Radushkevich (D-R) adsorption isotherm model:

$$q_e = q_s e^{-\beta_D \epsilon^2} \tag{11}$$

where $\beta_D$ is a constant related to the adsorption energy ($mol^2\ kJ^{-2}$) and $\varepsilon$ is the Polanyi potential ($KJ\ mol^{-1}$) which is defined as

$$\varepsilon = RTln\left(1 + \frac{1}{C_e}\right) \tag{12}$$

where $T$ (K) is the temperature and $R$ ($J\ mol^{-1}K^{-1}$) represents the ideal gas constant (Zhou et al. 2021).

The D-R model was developed taking in consideration the effect of the porous structure of the materials on the adsorption, assuming that the process is related to micropore volume filling rather than layer-by-layer adsorption onto pore walls (Hu and Zhang 2019).

The Krishnamurti isotherm model, which has been recently proved to fit S-shaped equilibrium data of water contaminants (Chu 2021), is reported in Eq. (13)

$$q = \frac{N_0}{\left(1 + K_2\, e^{-K_1 C_e}\right)} \tag{13}$$

where $N_0$ ($mg\ g^{-1}$) is the total amount of adsorbable molecules per unit mass of adsorbent, $K_1$($L\ mg^{-1}$) and $K_2$ are constants.

The Krishnamurti adsorption model assumes that the uptake of the adsorbate follows a co-operative adsorption mechanism where previously adsorbed molecules facilitate the adsorption of more molecules in neighbouring positions.

The parameters resulting from the fit of the experimental data for every isotherm model considered in this study are reported in Table 2. It can be seen that Y zeolite has a higher adsorption capacity than ZSM-5.

For both zeolites, the Langmuir, Shifted Langmuir and Freundlich models are not suitable to describe the experimental data, whereas the Sips, Jovanovich-Freundlich, Dubinin-Radushkevich and Krishnamurti models provide a better description of the data trend ($R^2 > 0.98$).

The Sips isotherm model is a combination of the Freundlich and Langmuir models, the good fit of the experimental data for both adsorbent materials obtained with this equation may be due to the hybrid nature of the model, which can describe a wide range of adsorbate concentrations (Ahmed and Dhedan 2012). The Sips model (also known as the Langmuir – Freundlich model) assumes a Gaussian-like distribution of the energy (Pérez-Botella et al. 2022). Additionally, it has been reported that the Sips model is the most appropriate, three-parametric isotherm used for monolayer adsorption of surfactant (Kalam et al. 2021).

With the Dubinin-Radushkevich, useful information can be obtained calculating the mean adsorption energy $E$ ($kJ\ mol^{-1}$) as follows:

$$E = \frac{1}{\sqrt{2\beta}} \tag{14}$$

When $E$ is below 8, the adsorption is mainly characterised by a physical mechanism, whereas if $8 < E < 16$, the uptake involves mostly chemisorption (Eeshwarasinghe et al. 2018; Zhou et al. 2021). $E$ values calculated using Eq. (14) were 0.40 and 0.39 for the zeolites ZSM-5 and Y, respectively, suggesting that the uptake is mainly governed by a physical mechanism. Similar behaviours had been found for the adsorption of organic substances onto bamboo charcoal (Fu et al. 2012) and polycyclic aromatic hydrocarbons on granular activated carbon from water matrices (Eeshwarasinghe et al. 2018). Therefore, the

**Table 2** Isotherm parameters, with confidence intervals at 95%, obtained with the adsorption isotherm models (eqs. 6–11, 13) for ZSM-5 and Y zeolites

| Isotherm model | | Zeolite ZSM-5 | Zeolite Y |
|---|---|---|---|
| Langmuir | $q_s$ | 106.5 ± 28.44 | 261.6 ± 71.10 |
| | $b$ | 0.04268 ± 0.024 | 0.01466 ± 0.011 |
| | $R^2$ | 0.8905 | 0.7756 |
| | SSE | 1891 | 1.80E + 04 |
| Shifted Langmuir | $q_s$ | 90.71 ± 13.87 | 262.2 ± 29.50 |
| | $b_{sh}$ | 0.08028 ± 0.033 | 0.01565 ± 5.49e-03 |
| | $C_{sh}$ | 2.8 | 9.16 ± 5.00 |
| | $R^2$ | 0.9351 | 0.9643 |
| | SSE | 1120 | 2866 |
| Freundlich | $K_F$ | 7.947 ± 4.45 | 17.8 ± 12.06 |
| | $n$ | 1.7504 ± 0.16 | 2.2543 ± 0.13 |
| | $R^2$ | 0.8119 | 0.8549 |
| | SSE | 3246 | 1.16E + 04 |
| Sips | $q_s$ | 66.16 ± 1.65 | 208.7 ± 8.45 |
| | $b_s$ | 0.1073 ± 4.15e-03 | 0.01871 ± 1.24e-03 |
| | $\beta_s$ | 3.773 ± 0.51 | 2.322 ± 0.39 |
| | $R^2$ | 0.9944 | 0.9919 |
| | SSE | 96.53 | 650.2 |
| Jovanovich-Freundlich | $q_s$ | 64.9 ± 1.46 | 201.9 ± 9.45 |
| | $a$ | 0.09352 ± 4.15e-03 | 0.01489 ± 1.47e-03 |
| | $\nu$ | 2.816 ± 0.37 | 1.582 ± 0.33 |
| | $R^2$ | 0.9943 | 0.9818 |
| | SSE | 99.2 | 1462 |
| Dubinin-Radushkevich | $q_s$ | 70.45 ± 3.26 | 206.9 ± 5.70 |
| | $\beta_D$ | 3.092 ± 1.26e + 07 | 3.22 ± 1.79e + 07 |
| | $c$* | 4.874 ± 1.98e + 07 | 24.21 ± 6.72e + 07 |
| | $R^2$ | 0.9872 | 0.9922 |
| | SSE | 221.2 | 626.6 |
| Krishnamurti | $N_0$ | 64.86 ± 1.3 | 196.6 ± 10.6 |
| | $K_2$ | 81.45 ± 39.42 | 16.59 ± 13.58 |
| | $K_1$ | 0.4707 ± 0.0582 | 0.05254 ± 0.01530 |
| | $R^2$ | 0.9934 | 0.9646 |
| | SSE | 98.22 | 2859 |

*c = RT

results of the isotherm model fitting indicate a monolayer adsorption of p-HBA onto zeolites with a non-uniform distribution of adsorption energies.

### 3.2.2 pH Influence

p-HBA has a hydroxyl group with a $pK_a$ of 7.61, thus, according to the pH of the aqueous solution, the molecule can be present in the protonated and deprotonated form in different proportions.

The influence of pH on the adsorption of p-HBA onto zeolites was investigated and was carried out through the determination of the adsorbed quantity at the equilibrium ($q_e$) at different pH values, between 4 and 10 (Fig. SM4); this pH interval was selected because water bodies normally have a pH within this range, and for very acidic pHs zeolites undergo degradation. For pHs from 4 to 7 the quantity of p-HBA adsorbed does not vary significantly; but, for pH values higher than 7, $q_e$ decreases notably, approaching zero value at a pH of 10. For pH values lower than the pKa, p-HBA is mainly present in the protonated form, and the adsorption onto the zeolite is favoured by the positive interactions with the framework of the adsorbent material. Whereas, for pH higher than the pKa, p-HBA is mainly present in the deprotonated form carrying a negative charge which interacts repulsively with the also negatively charged zeolite framework, resulting in a decrease of the quantity of p-HBA adsorbed. It has already been observed that when the pH increases above their pKa, the adsorption of phenolic compounds on zeolites decreases (Tri et al. 2020).

To better understand the influence of pH on the adsorption process, adsorption isotherms of the zeolites towards p-HBA were determined at three different pH values below the $pK_a$, in particular 3.5, 5 and 7, as presented in Fig. 3 for zeolite ZSM-5. As it can be seen in Fig. 3, independently from the pH value of the solution, the isotherms show the same shape reaching a saturation capacity value of about 60 mg $g^{-1}$; however, the curve is shifted towards higher adsorbate concentrations in solution as the pH increases, resulting in a smaller uptake compared to more acidic conditions; a similar behaviour was observed for zeolite Y.

## 3.3 Competition between p-HBA and TOL in the Adsorption onto ZSM-5

To investigate possible competitive behaviour between the natural compound p-HBA and the contaminant TOL on the uptake on zeolite ZSM-5, adsorption experiments were performed with binary mixtures containing both substances in different concentrations; in this case, the Sips isotherm model was utilised to fit the experimental data because it describes best the behaviour of the material towards the adsorption of both substances. Adsorption isotherms of p-HBA in the presence of TOL in different constant concentrations in solution

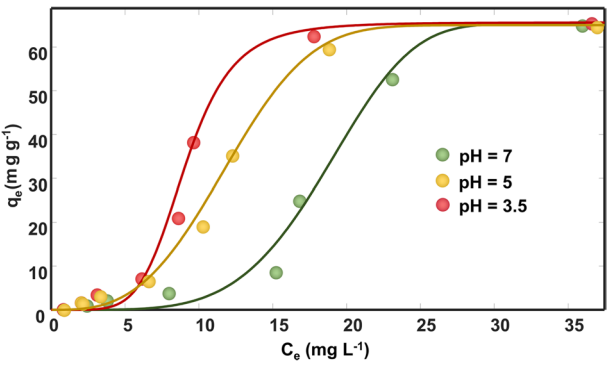


**Fig. 3** Isotherm experimental data of p-HBA on zeolite ZSM-5 at different pHs

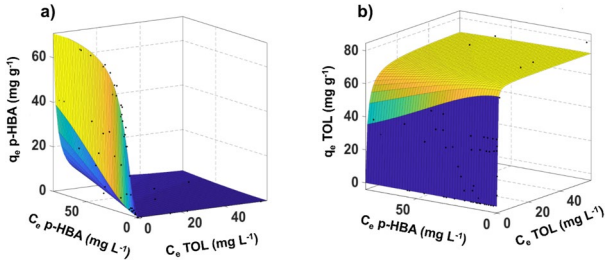


**Fig. 4** Nonlinear fitting (Sips isotherm model) of the adsorbed amount ($q_e$) on zeolite ZSM-5 of (**a**) p-HBA and (**b**) TOL from two-component aqueous solutions of p-HBA and TOL

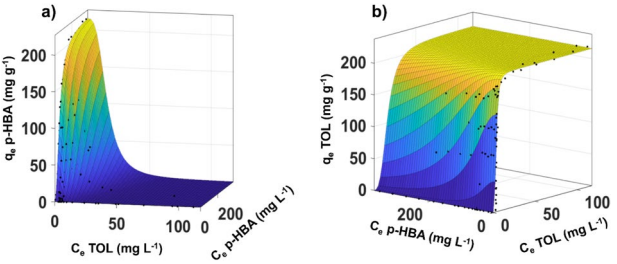


**Fig. 5** Nonlinear fitting (Sips isotherm model) of the adsorbed amount ($q_e$) on zeolite Y of (**a**) p-HBA and (**b**) TOL from two-components aqueous solutions of p-HBA and TOL

have been determined (Fig. 4). ZSM-5 shows a high saturation capacity towards p-HBA in absence of TOL; when TOL is added to the aqueous solution, the saturation capacity of the zeolite towards the natural compound decreases as the contaminant concentration increases (Fig. 4a). On the other hand, when the quantity of TOL adsorbed is considered from binary solutions containing both TOL and p-HBA, the $q_e$ of the contaminant is not significantly influenced, even when the natural substance is present in high concentrations (Fig. 4b).

To further investigate the selectivity of the zeolite towards the organic contaminant, adsorption kinetic experiments were performed to evaluate the uptake of TOL onto the zeolite previously saturated with p-HBA. As highlighted in Fig. SM5, the TOL concentration in the solution rapidly decreases, whereas the p-HBA concentration in the solution increases; these findings confirm the higher affinity of the zeolite towards TOL, whose adsorption is accompanied by the displacement of p-HBA molecules from the zeolite pores.

### 3.4 Competition between p-HBA and TOL in the Adsorption onto Y

The competitive behaviour between the natural compound and the organic contaminant was studied also for the zeolite Y. As for the case of zeolite ZSM-5, the selectivity of the adsorbent material was found to be higher for the contaminant rather than the lignin derived compound; in Fig. 5 the isotherms of p-HBA and TOL from binary solutions are presented.

Zeolite Y shows a large saturation capacity towards p-HBA when the organic contaminant is absent; when TOL is present in solution and its concentration increases, the saturation capacity of the zeolite Y towards the natural compound rapidly decreases (Fig. 5a). Similar findings were observed for the adsorption mixture of TOL and phenol in gas phase onto Y zeolite (Khalil et al. 2020).

If the uptake of TOL is considered, the saturation capacity of the adsorbent material is only slightly affected by the presence of p-HBA in the solution at any concentration (Fig. 5b).

The preference of both zeolites towards TOL rather than p-HBA can be attributed to the hydrophobic properties of TOL which allow stronger interactions with the high silica zeolite framework (TOL has a $\log K_{ow}$ of 2.73, whereas p-HBA has a $\log K_{ow}$ of 1.35); moreover, at neutral pH the partially dissociated nature of p-HBA leads to a lower uptake due to repulsive interactions between the dissociated form of the aldehyde and the negatively charged framework of the zeolite.

### 3.5 Thermal and Structural Characterisation of p-HBA-ZSM-5 and Y

Lattice parameters obtained by Rietveld structure refinements of ZSM-5 and Y zeolites are reported in Table 3. The crystal structure of both ZSM-5 and Y was markedly modified after the p-HBA adsorption; Rietveld structure refinements clearly indicated a lowering in symmetry: from *Fd-3 m* to *Fd-3* in Y zeolite and from monoclinic $P2_1/n$ to orthorhombic $P2_12_12_1$ in ZSM-5 (Table 3). The framework is not significantly modified by adsorption of p-HBA molecules. The tetrahedral T-O mean distances and the T-O-T angles adopt mean values in good agreement with those reported for the pure zeolites (<T–O> = 1.615 Å and <T–O-T> ranging from 126.6° to 150.1° in p-HBA-Y; average bond length = 1.615 Å; T-O-T angles ranging from 138.5 to 151.1° in as-synthesised Y); in p-HBA-ZSM-5 the T-O distances are in the range 1.587-1.600 Å, and T-O-T angles lie between 136.2° to 169.8°, with respect to the average bond length = 1.595 Å and bond angles ranging from 132.8° to 167.3° reported for the pristine ZSM-5.

The difference Fourier map for ZSM-5 shows p-HBA molecules distribution over two crystallographic independent sites, namely p-HBA1 and p-HBA2, analogously to the behaviour of TOL on ZSM-5 (Rodeghero et al. 2017). p-HBA1 site is located close to the straight channel, while p-HBA2 molecules are located at the intersection between straight and sinusoidal channels (see Table SM5). The most significant distances between

**Table 3** Lattice parameters for zeolites investigated before and after the adsorption of p-HBA, TOL and p-HBA-TOL mixture

| Space Group | ZSM-5<br>$P2_1/n$ | ZSM-5-*p*-HBA<br>$P2_12_12_1$ | ZSM-5-TOL<br>$P2_1/n$ | ZSM-5-*p*-HBA-TOL<br>$P2_1/n$ |
|---|---|---|---|---|
| *a (Å)* | 19.8999(5) | 19.9921(6) | 19.9062(1) | 19.9054(1) |
| *b (Å)* | 20.1174(6) | 19.9391(6) | 20.1176(1) | 20.1237(1) |
| *c (Å)* | 13.3892(4) | 13.3736(4) | 13.3926(1) | 13.3911(1) |
| *α (°)* | 90 | 90 | 90 | 90 |
| *β (°)* | 90.546(3) | 90 | 90.5446(11) | 90.5501(16) |
| *γ (°)* | 90 | 90 | 90 | 90 |
| *V (Å$^3$)* | 5359.9(3) | 5331.05(29) | 5363.01(12) | 5363.47(16) |
| | ***Y*** | ***Y-p-HBA*** | ***Y-TOL*** | ***Y-p-HBA-TOL*** |
| *Space Group* | *Fd-3 m* | *Fd-3* | *Fd-3* | *Fd-3* |
| *a = b = c(Å)* | 24.2590(1) | 24.27038(13) | 24.26739(7) | 24.26785(8) |
| *α = β = γ = 90°* | 90 | 90 | 90 | 90 |
| *V (Å$^3$)* | 14277.10(4) | 14296.50(13) | 14291.22(7) | 14292.03(8) |

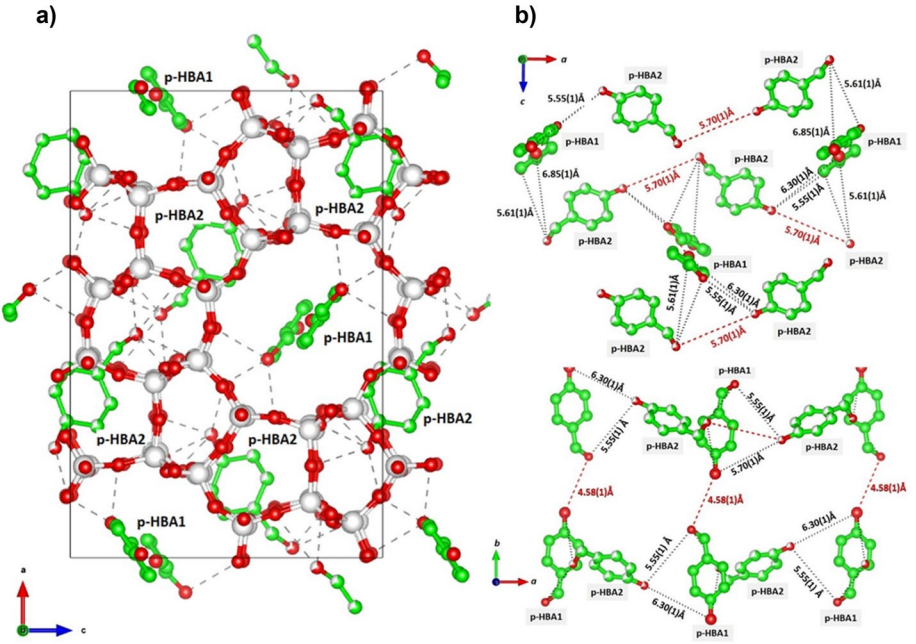


**Fig. 6** Adsorption sites of p-HBA in ZSM-5 structure (**a**); interaction between neighbouring p-HBA (**b**)

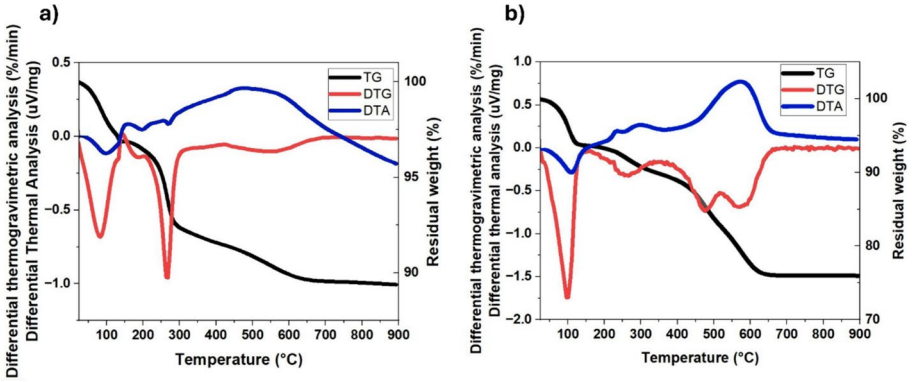


**Fig. 7** Simultaneous Thermogravimetry (black line), Differential Thermogravimetry (red line) and Differential Thermal analyses (blue line), in the temperature range from 25 to 900 °C, of ZSM-5 (a) and Y (b) zeolites loaded with p-HBA

the organics and the framework are reported in Table SM6. The molecular arrangement viewed along *b* axis is shown in Fig. 6. Both molecules are approximately planar, the average C-C distance in the benzene ring is 1.38 Å. The occupancy factors reveal that the loadings consist of 3.6 molecules per unit cell, equivalent to ~7.0% in weight (Table SM5). Therefore, structure refinement gave p-HBA content levels in good agreement with the weight loss registered by thermogravimetric measurements (Fig. 7a) and adsorption data (see Fig. 2a). In the TG curve, an initial weight loss below 100 °C is observed, which

can be possibly due to the desorption of water molecules and/or p-HBA molecules weakly bonded to the surface (about 5%). At higher temperature, the bond rupture and volatilisation of low molecular weight fragments of p-HBA occur (100–300℃). The next step (at 300–450 °C) corresponds to the complete p-HBA thermo-oxidative degradation accompanied by a broad exothermic peak registered in the DTA suggesting the release of CO and $H_2$. Above 650 °C, carbonaceous residues are expelled from the structure.

The distances between neighbouring p-HBA, defined as the internuclear distances between closest oxygen atoms of carboxyl and phenolic group, are 4.58 Å (p-HBA1-p-HBA1) and 5.70 Å (p-HBA2-p-HBA2), respectively. The shortest distance between neighbouring p-HBA1 and p-HBA2 molecules is 5.55 Å, which indicates the occurrence of end-to-end guest-guest interactions (Fig. 6b). At the same time, host-guest interactions are assumed, considering the p-HBA-framework oxygens intermolecular refined distances (Table SM6). Taken together, our results highlight that a complex network of linear p-HBA1-chains running parallel to the *b* axis is laterally branched to p-HBA2 molecules thus forming zig-zag oligomers interacting with the framework oxygens (Table SM6). Because of the larger pore openings (12MR instead of 10MR), the Y shape selectivity for p-HBA sorption distinctly differs from that of ZSM-5.

The refinement displays the occurrence of 23 p-HBA molecules per unit cell (~19.0% dry weight, dw %), in good accordance with the weight losses calculated from TGA analyses (Fig. 7b) and adsorption data (see Fig. 2b). These molecules occupy one crystallographic partially occupied site at the centre of the supercage, statistically assuming six different orientations generated by the presence of the 6-fold axis parallel to [111]. Difference Fourier maps generated using the GSAS suite show that along with the p-HBA, water molecules were also coadsorbed in the framework: particularly, ~28 molecules/u.c. (corresponding to ~3.0% dry weight, dw %) are detected (spread over four independent partially occupied sites W1, W2, W3 and W4) (Table SM7). In accordance with the Rietveld refinement, TG curve (Fig. 7b) highlights three major weight losses: the initial loss (~ 6.0 dw % zeolite, between 25 and 110 °C) is due to desorption of molecules retained on the surface, the last ones (20.5 dw % zeolite, between 110 and 900 °C) are caused by p-HBA thermo-oxidative degradation (accompanied by a broad exothermic peak registered in the DTA) and volatilisation of $H_2O$ molecules.

Water actively stabilises close-packing of p-HBA inside zeolite channels, the refined distances of the carbonyl oxygens from them amounting to 2.18 and 2.26 Å, respectively, indicating that the presence of water has relevant structural effects on the p-HBA arrangement (Fig. 8 and Table SM7). Water molecules involve guest p-HBA molecules into a complex hydrogen bond network forming oligomers (W4-W1-W2-W3-W2-W1-W4) strongly interacting with O1, O2 and O4 framework oxygens and acting at the same time as a bridge with oxygens atoms of carboxylic and phenolic group of p-HBA (Fig. 8). Similar findings have been reported by Bal'zhinimaev et al. (2019), the formation of p-HBA and water molecules clusters possibly account for the low adsorption of organics from dilute solutions (Pasti et al. 2018). Structural analysis evidenced multiple interactions corresponding to a non-uniform energy distribution in agreement with the isotherm model results.

The formation of water-organics complexes that can interact with the framework, leading to the stabilisation of the guest structures within the adsorbent porosity was also recently reported in literature (Arletti et al. 2012; Rodeghero et al. 2016; Pasti et al. 2018).

Variations in both the position and intensity of diffraction peaks are strongly evident after p-HBA adsorption, thus indicating changes on cell parameter values as well as on atomic parameters, such as positional coordinates x, y, z, isotropic temperature factor, etc. Powder patterns collected before and after adsorption of p-HBA-TOL mixtures are very

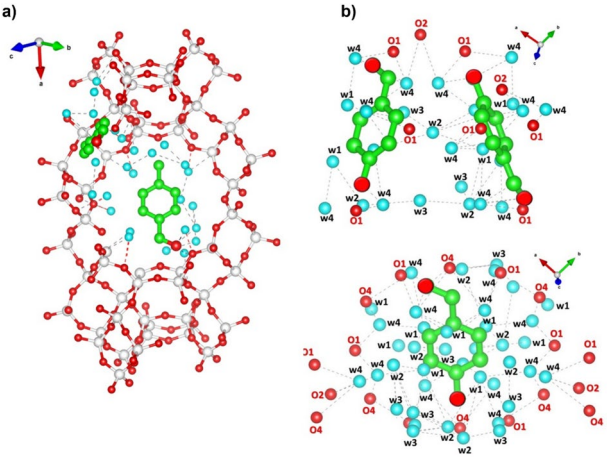


**Fig. 8** Adsorption sites of p-HBA in Y structure (**a**); interaction between p-HBA, water molecules and framework oxygens (**b**)

similar to those after only toluene adsorption (Fig. 9) in both zeolites. The monoclinic symmetry of the pristine ZSM-5 was preserved after p-HBA-TOL mixture adsorption: the presence of several doublets (i.e., $131+13-1$ and $311+31-1$, and $133+13-3$ and $313+31-3$) as well as the refined $\beta$ angle (Table 3) confirmed this assumption. In zeolite Y, the stronger affinity towards TOL in p-HBA-TOL binary mixtures was also suggested by the strong similarities between the powder patterns of both zeolites after TOL and p-HBA-TOL adsorption (Fig. 9), then confirmed by the refined unit cell parameters (Table 3). Besides, the DTA curves of TOL-Zeolite and p-HBA-TOL binary mixtures (Fig. 10) show an indistinguishable behaviour for both ZSM-5 and Y, thus proving the preferential uptake of TOL vs. p-HBA.

## 4 Conclusions

The present study elucidates p-HBA adsorption from aqueous solution on ZSM-5 and Y high silica zeolites. It has been found that both zeolites adsorb p-HBA, and the adsorption is influenced by pH, especially at low concentrations. The adsorption of p-HBA takes place within the porous structure of the zeolites and occurs through the formation of water-organics complexes which interact with the framework, stabilising the guest structures within the adsorbent material porosity. Adsorption experiments were conducted using binary mixtures of toluene and p-HBA at different concentrations, and the experimental data were fitted using competitive isotherm models. Our experimental findings revealed that the selectivity of ZSM-5 and Y high silica zeolites is higher for toluene. Furthermore, adsorption kinetic experiments were carried out to assess the uptake of toluene onto zeolite previously saturated with p-HBA. The results confirm the higher affinity of zeolites towards toluene, with its adsorption accompanied by the displacement of p-HBA molecules from the zeolite pores. Molecular-level investigations demonstrate that toluene and p-HBA in both zeolites compete for the occupancy of the same adsorption sites. Understanding

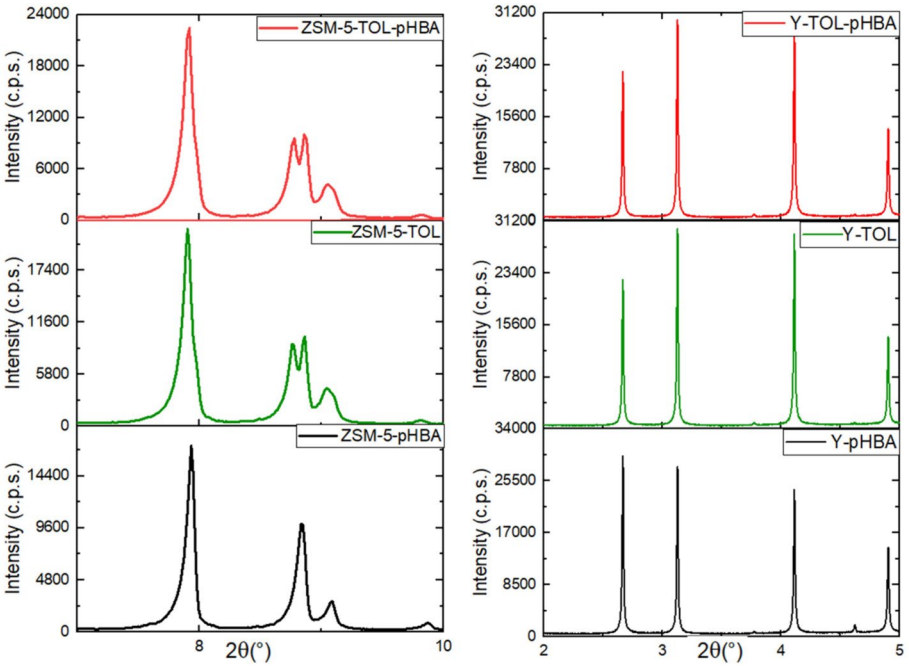


**Fig. 9** X-ray Powder Diffraction cascade plots of zeolites ZSM-5 and Y after p-HBA, TOL and p-HBA-TOL mixture adsorption, collected at room temperature in selected angular ranges. The strong similarities between the powder patterns of both zeolites after TOL and p-HBA-TOL contact confirmed the preferred adsorption of toluene in the mixture

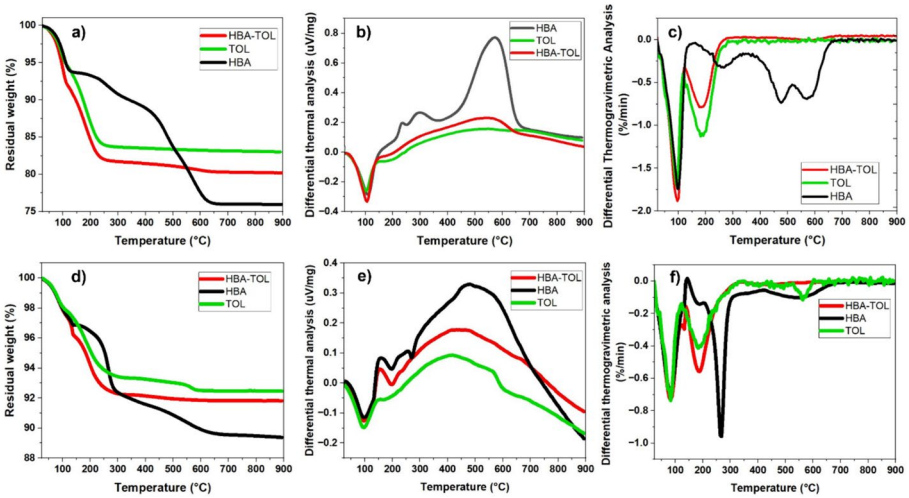


**Fig. 10** Simultaneous Thermogravimetry, Differential Thermal analyses and Differential Thermogravimetry, in the temperature range from 25 to 900 °C, of Y (a, b, c, respectively) and ZSM-5 (d, e, f, respectively) zeolites loaded with p-HBA, TOL and p-HBA-TOL mixture

competitive adsorption mechanisms is crucial for designing treatment plants for natural and wastewaters.

**Supplementary Information** The online version contains supplementary material available at https://doi.org/10.1007/s40710-024-00726-2.

**Acknowledgements** The Authors would like to thank Giuliana Magnacca of the University of Turin for helping us in the zeolites texture characterisation.

**Author Contributions** T.C. Writing - original draft, Visualisation, Investigation, Conceptualisation. M. M. Writing - original draft, Data curation, Investigation, Methodology. E. S. Data curation, Methodology. V.C. Investigation, Methodology, Visualisation. C. D. Data curation, Investigation. A. M. Supervision, Resources, Writing - review & editing. L. P. Supervision, Funding acquisition, Project administration, Resources, Writing – review & editing. All authors read and approved the final manuscript.

**Funding** Open access funding provided by Università degli Studi di Ferrara within the CRUI-CARE Agreement. The research leading to these results has received funding from PNRR MUR project ECS_00000033_ECOSISTER.

**Data Availability** No datasets were generated or analysed during the current study.

## Declarations

**Ethical** The current study did not include any human or animal subjects. Thus, this study is not subject to an ethics review committee and does not require any informed consent.

**Competing Interests** The authors declare no competing interests.



## References

Abas KM, Fathy NA (2024) Sodalite zeolitic materials produced from coal fly ash for removal of Congo red dye from aqueous solutions. Int J Environ Sci Technol 21:5165–5184. https://doi.org/10.1007/s13762-023-05347-0

Ahmed MJ, Dhedan SK (2012) Equilibrium isotherms and kinetics modeling of methylene blue adsorption on agricultural wastes-based activated carbons. Fluid Phase Equilib 317:9–14. https://doi.org/10.1016/j.fluid.2011.12.026

Almuhtaseb RM, Bhagyaraj S, Krupa I (2024) A concise review on BTEX remediation from aqueous solutions by adsorption. Emergent Mater 7:695–719. https://doi.org/10.1007/s42247-024-00640-1

Amrutha, Jeppu G, Girish CR et al (2023) Multi-component Adsorption isotherms: review and modeling studies. Environ Process 10:38. https://doi.org/10.1007/s40710-023-00631-0

Arletti R, Martucci A, Alberti A et al (2012) Location of MTBE and toluene in the channel system of the zeolite mordenite: Adsorption and host–guest interactions. J Solid State Chem 194:135–142. https://doi.org/10.1016/j.jssc.2012.04.024

Baerlocher C, Mccusker LB, Olson DH (2007) Atlas of Zeolite framework types. Elsevier Sci B V. 6th edn.https://doi.org/10.1016/B978-044453064-6/50187-0

Bal'zhinimaev BS, Paukshtis EA, Toktarev AV et al (2019) Effect of water on toluene adsorption over high silica zeolites. Micropor Mesopor Mater 277:70-7

Beckett R, Ranville J (2006) Chap. 17: Natural organic matter. In Interface Science in Drinking Water Treatment, Theory and Applications (vol 10). Elsevier Ltd. pp 299–215

Braschi I, Martucci A, Blasioli S et al (2016) Effect of humic monomers on the adsorption of sulfamethoxazole sulfonamide antibiotic into a high silica zeolite Y: an interdisciplinary study. Chemosphere 155:444–452. https://doi.org/10.1016/j.chemosphere.2016.04.008

Bujdák J (2020) Adsorption kinetics models in clay systems. The critical analysis of pseudo-second order mechanism. Appl Clay Sci 191:105630. https://doi.org/10.1016/j.clay.2020.105630

Chenet T, Sarti E, Costa V et al (2020) Influence of caffeic acid on the adsorption of toluene onto an organophilic zeolite. J Environ Chem Eng 8:104229. https://doi.org/10.1016/j.jece.2020.104229

Cheung CW, Porter JF, Mckay G (2001) Sorption kinetic analysis for the removal of cadmium ions from effluents using bone char. Water Res 35:605–612. https://doi.org/10.1016/S0043-1354(00)00306-7

Chi X, Zeng L, Du Y et al (2022) Adsorption of levofloxacin on natural zeolite: effects of ammonia nitrogen and humic acid. Water Sci Technol 85:2928–2944. https://doi.org/10.2166/wst.2022.121

Chu KH (2021) Fitting a little-known isotherm equation to S-shaped adsorption equilibrium data. Sep Purif Technol 259:118079. https://doi.org/10.1016/j.seppur.2020.118079

Eeshwarasinghe D, Loganathan P, Kalaruban M et al (2018) Removing polycyclic aromatic hydrocarbons from water using granular activated carbon: kinetic and equilibrium adsorption studies. Environ Sci Pollut Res 25:13511–13524. https://doi.org/10.1007/s11356-018-1518-0

Elovich S, Larinov O (1962) Theory of adsorption from nonelectrolyte solutions on solid adsorbents. Bulletin of the Academy of Sciences of the USSR. Div Chem Sci 11:198–203

Foo KY, Hameed BH (2010) Insights into the modeling of adsorption isotherm systems. Chem Eng J 156:2–10. https://doi.org/10.1016/j.cej.2009.09.013

Fu D, Zhang Y, Lv F et al (2012) Removal of organic materials from TNT red water by Bamboo Charcoal adsorption. Chem Eng J 193–194:39–49. https://doi.org/10.1016/j.cej.2012.03.039

Fuentes B, Mora M, de la L, Bol R et al (2014) Sorption of inositol hexaphosphate on desert soils. Geoderma 232–234:573–580. https://doi.org/10.1016/j.geoderma.2014.06.016

González-López ME, Laureano-Anzaldo CM, Pérez-Fonseca AA et al (2022) A critical overview of Adsorption models linearization: methodological and statistical inconsistencies. Sep Purif Rev 51:358–372. https://doi.org/10.1080/15422119.2021.1951757

Grant PG, Lemke SL, Dwyer MR, Phillips TD (1998) Modified Langmuir Equation for S-Shaped and Multisite Isotherm Plots. Langmuir 14:4292–4299. https://doi.org/10.1021/la971218a

Günay A, Arslankaya E, Tosun İ (2007) Lead removal from aqueous solution by natural and pretreated clinoptilolite: adsorption equilibrium and kinetics. J Hazard Mater 146:362–371. https://doi.org/10.1016/j.jhazmat.2006.12.034

Guo X, Wang J (2019) A general kinetic model for adsorption: theoretical analysis and modeling. J Mol Liq 288:111100. https://doi.org/10.1016/j.molliq.2019.111100

Hincapié–Upegui D, Pemberthy Mendoza D, Peñuela GA (2024) Formation of disinfection by-products and biodegradability of dissolved organic matter fractions from a tropical high-mountain reservoir. Int J Environ Sci Technol 21:2559–2574. https://doi.org/10.1007/s13762-023-05139-6

Ho Y-S (2006) Second-order kinetic model for the sorption of cadmium onto tree fern: a comparison of linear and non-linear methods. Water Res 40:119–125. https://doi.org/10.1016/j.watres.2005.10.040

Hu Q, Zhang Z (2019) Application of Dubinin–Radushkevich isotherm model at the solid/solution interface: a theoretical analysis. J Mol Liq 277:646–648. https://doi.org/10.1016/j.molliq.2019.01.005

IARC (1999) IARC monographs on the evaluation of carcinogenic risks to humans volume 73: some chemicals that cause tumors of the kidney or urinary bladder in rodents and some other substances. IARC, Lyon. (France)

Jacangelo JG, DeMarco J, Owen DM, Randtke SJ (1995) Selected processes for removing NOM: an overview. J Am Water Works Assoc 87:64–77. https://doi.org/10.1002/j.1551-8833.1995.tb06302.x

Jiang J, Han J, Zhang X (2020) Nonhalogenated Aromatic DBPs in drinking Water Chlorination: a gap between NOM and Halogenated aromatic DBPs. Environ Sci Technol 54:1646–1656. https://doi.org/10.1021/acs.est.9b06403

Kalam S, Abu-Khamsin SA, Kamal MS, Patil S (2021) Surfactant Adsorption isotherms: a review. ACS Omega 6:32342–32348. https://doi.org/10.1021/acsomega.1c04661

Khalil I, Jabraoui H, Lebègue S et al (2020) Biofuel purification: coupling experimental and theoretical investigations for efficient separation of phenol from aromatics by zeolites. Chem Eng J 402:126264. https://doi.org/10.1016/j.cej.2020.126264

Lagergren S (1898) Zur Theorie Der Sogenannten adsorption gelöster stoffe, Kungliga Svenska Vetenskapsakademiens. Kungliga Svenska Vetenskapsakademiens Handlingar 24:1–39

Larson AC, Von Dreele RB (2004) General Structure Analysis System (GSAS). Los Alamos National Laboratory, Los Alamos, NM (USA). Technical Report LAUR 86:748

Lima EC, Sher F, Guleria A et al (2021) Is one performing the treatment data of adsorption kinetics correctly? J Environ Chem Eng 9:104813. https://doi.org/10.1016/j.jece.2020.104813

Ma X, Liu X, Anderson DP, Chang PR (2015) Modification of porous starch for the adsorption of heavy metal ions from aqueous solution. Food Chem 181:133–139. https://doi.org/10.1016/j.foodchem.2015.02.089

Mancinelli M, Stevanin C, Ardit M et al (2022) PFAS as emerging pollutants in the environment: a challenge with FAU type and silver-FAU exchanged zeolites for their removal from water. J Environ Chem Eng 10:108026. https://doi.org/10.1016/j.jece.2022.108026

Marin P, Borba CE, Módenes AN et al (2014) Determination of the mass transfer limiting step of dye adsorption onto commercial adsorbent by using mathematical models. Environ Technol 35:2356–2364. https://doi.org/10.1080/09593330.2014.904445

Mathew RA, Mowla M, Shakiba S et al (2024) Prediction of nanoparticle photoreactivity in mixtures of Surface foulants requires kinetic (Non-equilibrium) adsorption considerations. Environ Sci Technol 58:8542–8553. https://doi.org/10.1021/acs.est.3c09677

Matilainen A, Gjessing ET, Lahtinen T et al (2011) An overview of the methods used in the characterisation of natural organic matter (NOM) in relation to drinking water treatment. Chemosphere 83:1431–1442. https://doi.org/10.1016/j.chemosphere.2011.01.018

McLintock IS (1967) The Elovich equation in Chemisorption Kinetics. Nature 216:1204–1205. https://doi.org/10.1038/2161204a0

Mitch WA, Richardson SD, Zhang X, Gonsior M (2023) High-molecular-weight by-products of chlorine disinfection. Nat Water 1:336–347. https://doi.org/10.1038/s44221-023-00064-x

Molé RA, Velosa AC, Carey GR et al (2024) Groundwater solutes influence the adsorption of short-chain perfluoroalkyl acids (PFAA) to colloidal activated carbon and impact performance for in situ groundwater remediation. J Hazard Mater 474:134746. https://doi.org/10.1016/j.jhazmat.2024.134746

Monte Blanco SPD, Scheufele FB, Módenes AN et al (2017) Kinetic, equilibrium and thermodynamic phenomenological modeling of reactive dye adsorption onto polymeric adsorbent. Chem Eng J 307:466–475. https://doi.org/10.1016/j.cej.2016.08.104

Park Y, Sun Z, Ayoko GA, Frost RL (2014) Bisphenol A sorption by organo-montmorillonite: implications for the removal of organic contaminants from water. Chemosphere 107:249–256. https://doi.org/10.1016/j.chemosphere.2013.12.050

Parniske J, Atallah Al-asad H, Qian J, Morck T (2024) Modelling competitive adsorption of organic micropollutants onto powdered activated carbon in continuous stirred tank reactors for advanced wastewater treatment. Water Res 258:121806. https://doi.org/10.1016/j.watres.2024.121806

Pasti L, Rodeghero E, Beltrami G et al (2018) Insights into Adsorption of Chlorobenzene in high silica MFI and FAU zeolites gained from Chromatographic and Diffractometric Techniques. Minerals 8:80. https://doi.org/10.3390/min8030080

Pérez-Botella E, Valencia S, Rey F (2022) Zeolites in adsorption processes: state of the art and future prospects. Chem Rev 122:17647–17695. https://doi.org/10.1021/acs.chemrev.2c00140

Pignatello JJ, Kwon S, Lu Y (2006) Effect of Natural Organic substances on the Surface and Adsorptive Properties of Environmental Black Carbon (Char): attenuation of Surface Activity by Humic and Fulvic acids. Environ Sci Technol 40:7757–7763. https://doi.org/10.1021/es061307m

Plazinski W, Rudzinski W, Plazinska A (2009) Theoretical models of sorption kinetics including a surface reaction mechanism: a review. Adv Colloid Interface Sci 152:2–13. https://doi.org/10.1016/j.cis.2009.07.009

Quiñones I, Guiochon G (1996) Derivation and application of a Jovanovic-Freundlich Isotherm Model for single-component adsorption on heterogeneous surfaces. J Colloid Interface Sci 183:57–67. https://doi.org/10.1006/jcis.1996.0518

Rodeghero E, Martucci A, Cruciani G et al (2016) Kinetics and dynamic behaviour of toluene desorption from ZSM-5 using in situ high-temperature synchrotron powder X-ray diffraction and chromatographic techniques. Catal Today 277:118–125. https://doi.org/10.1016/j.cattod.2015.11.031

Rodeghero E, Pasti L, Sarti E et al (2017) Temperature-Induced Desorption of Methyl tert-butyl ether confined on ZSM-5: an in situ Synchrotron XRD Powder Diffraction Study. Minerals 7:34. https://doi.org/10.3390/min7030034

Scheufele FB, Módenes AN, Borba CE et al (2016) Monolayer–multilayer adsorption phenomenological model: kinetics, equilibrium and thermodynamics. Chem Eng J 284:1328–1341. https://doi.org/10.1016/j.cej.2015.09.085

Suzaki PYR, Munaro MT, Triques CC et al (2017) Biosorption of binary heavy metal systems: phenomenological mathematical modeling. Chem Eng J 313:364–373. https://doi.org/10.1016/j.cej.2016.12.082

Toby BH (2001) EXPGUI, a graphical user interface for GSAS. J Appl Crystallogr 34:210–213. https://doi.org/10.1107/S0021889801002242

Tri NLM, Thang PQ, Van Tan L et al (2020) Removal of phenolic compounds from wastewaters by using synthesized Fe-nano zeolite. J Water Process Eng 33:101070. https://doi.org/10.1016/j.jwpe.2019.101070

Turk Sekulic M, Boskovic N, Milanovic M et al (2019) An insight into the adsorption of three emerging pharmaceutical contaminants on multifunctional carbonous adsorbent: mechanisms, modelling and metal coadsorption. J Mol Liq 284:372–382. https://doi.org/10.1016/j.molliq.2019.04.020

Wang Q, Lechtenfeld OJ, Rietveld LC et al (2024) How aromatic dissolved organic matter differs in competitiveness against organic micropollutant adsorption. Environ Sci Ecotechnol 21:100392. https://doi.org/10.1016/j.ese.2024.100392

Zhou Y, Li Y, Liu D et al (2021) Adsorption optimization of uranium(VI) onto polydopamine and sodium titanate co-functionalized MWCNTs using response surface methodology and a modeling approach. Colloids Surf Physicochem Eng Asp 627:127145. https://doi.org/10.1016/j.colsurfa.2021.127145

Zhu C, Nie Y, Zhao S et al (2022) Constructing surface micro-electric fields on hollow single-atom cobalt catalyst for ultrafast and anti-interference advanced oxidation. Appl Catal B 305:121057. https://doi.org/10.1016/j.apcatb.2021.121057

Zuo X, Qian C, Ma S, Xiong J (2020) Sulfonamide antibiotics sorption by high silica ZSM-5: effect of pH and humic monomers (vanillin and caffeic acid). Chemosphere 248:126061. https://doi.org/10.1016/j.chemosphere.2020.126061